# Toward intrinsic functionalities of bilayered ruthenate $Sr_3Ru_2O_7$

R. Ciancio,[1,2,*] J. Börjesson,[2] H. Pettersson,[2] R. Fittipaldi,[1] D. Zola,[1] A. Vecchione,[1] M. Polichetti,[1] S. Kittaka,[3] Y. Maeno,[3] S. Pace,[1] and E. Olsson[2]

[1]*CNR-INFM SuperMat Regional Laboratory and Physics Department "E. R. Caianiello," University of Salerno, Baronissi, 84081 Salerno, Italy*

[2]*Department of Applied Physics, Microscopy and Microanalysis, Chalmers University of Technology, 412 96 Göteborg, Sweden*

[3]*Department of Physics, Graduate School of Science, Kyoto University, Kyoto 606-8502, Japan*

(Received 28 April 2009; revised manuscript received 13 July 2009; published 27 August 2009)

Polymorphic materials are known for being prone to intergrowth. Remarkable examples are strontium ruthenates whose properties are dramatically tuned by impurities and disorder. In particular, $Sr_3Ru_2O_7$ shows a strong variation in transport and magnetic properties depending on synthesis process. It is therefore crucial to correlate atomic structure and properties to identify the functionalities of individual nanostructural constituents. We report a comparative study between $Sr_3Ru_2O_7$ crystals grown as single phase and in $Sr_3Ru_2O_7$-$Sr_2RuO_4$ eutectics. Our analysis by transmission electron microscopy reveals that $Sr_3Ru_2O_7$ domains of the eutectic have a significantly lower level of impurities compared to $Sr_3Ru_2O_7$ single-phase crystals, where intergrowths of $Sr_4Ru_3O_{10}$ and $SrRuO_3$ phase are seen. This is confirmed by magnetic measurements. These results identify the eutectic solidification as a fruitful way to grow highly pure crystals of polymorphic materials which, in combination with recent technological developments allowing the extraction of embedded features of crystals, opens a pathway for understanding of their physical properties and applications.

DOI: 10.1103/PhysRevB.80.054110 PACS number(s): 74.70.Pq, 68.37.Og, 81.30.−t

## I. INTRODUCTION

Over the last decades, perovskite oxides in the Ruddlesden-Popper (R-P) series have been a major focus as they exhibit a wealth of exceptional properties such as high-temperature superconductivity in cuprates and colossal magnetoresistance in manganites. Among them, the 4*d*-electron-based $Sr_{n+1}Ru_nO_{3n+1}$ strontium ruthenates attracted widespread interest for the profound $n$ dependence of their physical properties providing an ideal playground to study new forms of order in materials with strong electron-electron interactions. Due to the competition between the conduction band width $W$ and the Coulomb interaction $U$,[1] these materials exist in a narrow range across the metal/insulator boundary ($U/W \approx 1$), so that small structural variations, diluted doping, pressure changes, and alterations of crystal structures can enable pronounced changes in both physical properties and ground-state behavior. In general, all the strontium ruthenates are metallic when they are grown in their stoichiometric forms and inclined to be magnetically ordered but small changes in either the crystal structure or the phase purity can switch their ground states all the way from correlated electron insulators to high-conductivity metals.[2–4] A great exception is represented by the $n=1$ member, the single-layered $Sr_2RuO_4$, which is a paramagnet displaying an unconventional spin-triplet superconductivity near 1.5 K.[2] In contrast to most of the superconducting materials, the superconducting state in $Sr_2RuO_4$ is sensitively suppressed also by nonmagnetic impurities or defects.[5] Indeed, the achievement of high-quality single crystals with remarkably low residual resistivity is crucial to observe the superconducting state in $Sr_2RuO_4$ at 1.5 K.[6] With regard to the synthesis of the intermediate oxides of the $Sr_{n+1}Ru_nO_{3n+1}$ series, the chemical phase diagram[7] and the Ru evaporation at high temperatures considerably restrict the achievement of highly pure single crystals of the $n=2$ member, the double-layered $Sr_3Ru_2O_7$. So far, although impressive advances have been made in the fabrication of single crystals of $Sr_3Ru_2O_7$, their transport and magnetic properties are strongly related to the levels of disorder in which they are grown.[8–10] $Sr_3Ru_2O_7$ was first found to be antiferromagnetic,[11] later reported as an itinerant ferromagnet,[12] then as an enhanced paramagnetic metal with a changeover from paramagnetism to ferromagnetism under uniaxial pressure,[13] lately claimed as a metamagnet with quantum criticality.[10] An impurity-induced transition to a Mott-insulator ground state has been found in single crystals of $Sr_3Ru_2O_7$ doped by only a few percent of Mn at the Ru site.[14] Moreover, a superconducting state has been very recently measured in $Sr_3Ru_2O_7$ grown in $Sr_3Ru_2O_7$-$Sr_2RuO_4$ eutectic crystals by flux-feeding floating-zone technique.[15–18] Several pictures have been proposed to explain this unusual behavior such as a proximity effect[16] or an exotic pairing coming from $Sr_2RuO_4$ inclusions finely dispersed in the $Sr_3Ru_2O_7$ domain.[18] Due to the lack of a detailed microstructural investigation aimed at clarifying the occurrence of spurious phases, a conclusive picture on the intrinsic properties of $Sr_3Ru_2O_7$ is still missing. Recurrent intergrowths of R-P layers with other $n$ values have been observed by transmission electron microscopy (TEM) in $Sr_3Ru_2O_7$ polycrystals[19] and thin films.[20] This phenomenon is typical of layered materials with polymorphism[21,22] and sensitively affects the corresponding transport/magnetic properties.[23] In case of growth of $Sr_3Ru_2O_7$ crystals, three different phases, i.e., $Sr_2RuO_4$, $Sr_4Ru_3O_{10}$, and $SrRuO_3$, can solidify due to their compatible Gibbs formation energies and to the Ru excess used to compensate its evaporation during the growth which may yield the solidification of the last two phases. The analysis on the structure at atomic level by TEM of $Sr_3Ru_2O_7$ is therefore crucial to shed light on its intrinsic properties and on the interplay between processing

 

parameters, nanostructures, and transport/magnetic properties.

In this work, we report on a comparative study on the nanostructures of the $Sr_3Ru_2O_7$ single-phase crystals (SPC) and of the $Sr_3Ru_2O_7$ region of a $Sr_3Ru_2O_7$-$Sr_2RuO_4$ eutectic crystal (EC). Furthermore, to establish the correlation between structure and functionalities, we studied the magnetic properties of both the $Sr_3Ru_2O_7$ SPC and the $Sr_3Ru_2O_7$-$Sr_2RuO_4$ EC in low magnetic fields.

## II. SAMPLE AND EXPERIMENT

The $Sr_3Ru_2O_7$ SPC and the $Sr_3Ru_2O_7$-$Sr_2RuO_4$ EC have been grown by flux feeding floating-zone technique with Ru self-flux, using a commercial image furnace equipped with double-elliptical mirrors and two 2.0 kW halogen lamps (NEC Machinery, model SC-K15HD-HP). An off-stoichiometric ratio $k_{SPC}=1.6$ and $k_{EC}=1.45$, respectively [where $k=2N(\mathrm{Ru})/N(\mathrm{Sr})$, $N(\mathrm{Ru})$ and $N(\mathrm{Sr})$ being the mol fraction for Sr and Ru] was used to compensate the Ru evaporation during the crystal growth.[15] During the eutectic solidification, the $Sr_3Ru_2O_7$ and $Sr_2RuO_4$ phases solidify along the *b* direction in an ordered pattern consisting of alternating lamellae of thickness ranging from 60 to 200 $\mu$m piled up along the *c* direction. From polarized light optical microscopy investigation, the $Sr_3Ru_2O_7$-$Sr_2RuO_4$ EC result in about 40 percent of volume fractions of $Sr_2RuO_4$ and about 60 percent of $Sr_3Ru_2O_7$ corresponding to a final mean ratio $k_f=1.2$. For the $Sr_3Ru_2O_7$-$Sr_2RuO_4$ EC crystal the decrease from the initial value ($k_{EC}=1.45$) is a consequence of the Ru evaporation during the growth leading, at the steady state of the growth, to the $k_f=1.2$ mean ratio in the liquid nearby the solid-liquid interface. X-ray analysis showed only the presence of the $Sr_2RuO_4$ and $Sr_3Ru_2O_7$ phases which are fully aligned in the crystallographic directions.[15] Rietveld analysis of powdered eutectic crystals confirmed the previously determined ratio between the two phases.

The microstructure of the crystals was explored using a Leo Ultra 55 field emission gun scanning electron microscope (SEM) with attached Oxford INCA Energy 300 energy-dispersive x-ray spectroscopy (EDS) system. The EDS analyses were carried out operating the microscope at 20 kV and at 10 mm working distance using an aperture size of 30 $\mu$m and a probe current of 5 nA.

The TEM studies were performed using a Philips CM 200 field emission gun TEM operated at 200 kV with an attached Link ISIS EDS system and a Gatan Imaging Filter. TEM specimens were extracted using a Fei Strata 235 DualBeam combined SEM and focused ion beam (FIB) instrument. 100-nm-thick TEM foils were thus obtained by a FIB-SEM lift-out procedure and further thinned down to electron transparency by a Gatan Precision Ion Polishing System equipped with two Ar sources.

The magnetic measurements have been performed by means of a vibrating sample magnetometer (VSM) inserted in a Quantum Design, Inc. USA, physical property measurement system (PPMS) 6000, a system with a cryostat equipped with a superconducting magnet. The equipment can measure the magnetic moment ($m$) in the temperature range from 2 to 400 K and the magnetic field $H_0$ can ramp from −90 kOe to 90 kOe. The dc susceptibility is given by $\chi = m/(H_0 \times P)$, where $P$ is the sample mass.

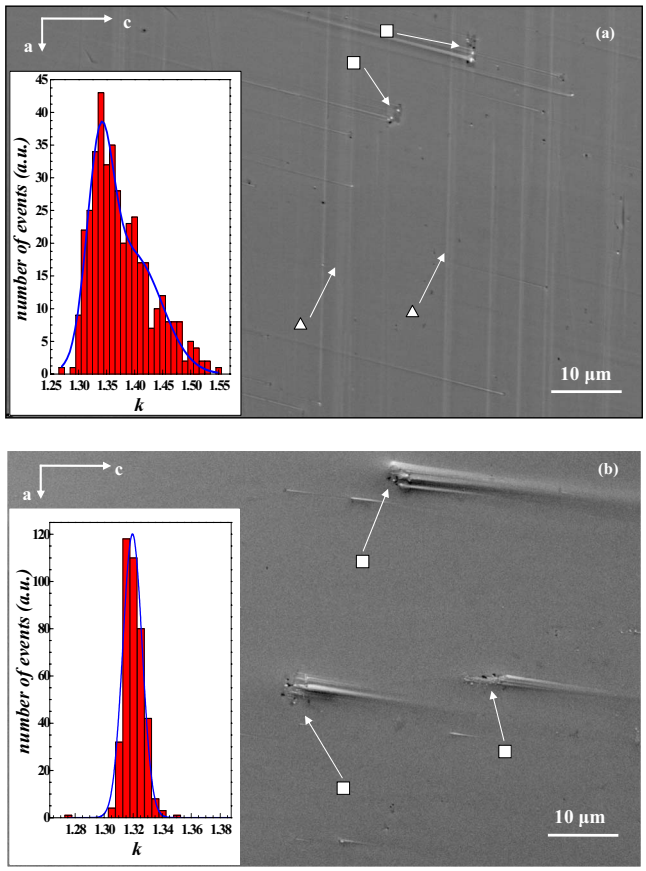


FIG. 1. (Color online) Backscattered SEM images taken in the *a-c* plane of (a) a $Sr_3Ru_2O_7$ single crystal showing layered defects of bright contrast (arrows with triangles) and clustered defects (arrows with squares) dispersed in the dark contrast $Sr_3Ru_2O_7$ matrix and (b) the $Sr_3Ru_2O_7$ region of a $Sr_3Ru_2O_7$-$Sr_2RuO_4$ eutectic crystal, in which the clustered defects are indicated by arrows with squares. In the insets, the histograms representing the number of EDS analyses versus different values of $k=2N(\mathrm{Ru})/N(\mathrm{Sr})$ obtained for each system. The blue lines are guides to the eyes.

## III. RESULTS AND DISCUSSION

The morphological characterization carried out by SEM on $Sr_3Ru_2O_7$ SPC revealed the presence of two kinds of defects. The SEM micrograph of Fig. 1(a), taken in the *a-c* plane of a well-polished $Sr_3Ru_2O_7$ SPC by back-scattered electrons, shows the occurrence in the $Sr_3Ru_2O_7$ matrix of both layered spurious phases (stripes of bright contrast) and irregularly shaped clusters with incorporated nanosized bright contrast particles.

The clusters of about $(5\times5)$ $\mu m^2$ size are randomly dispersed throughout the microstructure over distances ranging from 10 to 50 $\mu$m. The straight marks running from the clusters are due to the polishing procedure and indicate that the embedded particles are harder than the surrounding matrix. On the contrary, the same analysis performed on the

$Sr_3Ru_2O_7$ domain of the $Sr_3Ru_2O_7$-$Sr_2RuO_4$ EC [Fig. 1(b)] revealed a homogeneous microstructure where no layered defects are seen, even at high magnification. Clusters similar to those observed in the $Sr_3Ru_2O_7$ SPC case are detectable. The presence of such defects indicates the occurrence of local changes in composition with a significantly higher purity of the $Sr_3Ru_2O_7$ domain of the $Sr_3Ru_2O_7$-$Sr_2RuO_4$ EC compared to the $Sr_3Ru_2O_7$ SPC. To statistically explore the chemical composition of the two systems, a grid of [40 (along $c$-axis) $\times$ 10 (along $a$-axis)] fine probe energy-dispersive spectroscopy spots analysis was traced over regions of approximately $(150 \times 100)$ $\mu m^2$. The amounts of strontium, ruthenium, and oxygen were determined at each spot and converted into the equivalent mol fractions. The EDS data corresponding to each system are represented in the histograms of the insets of Fig. 1, where the number of events versus the corresponding value of $k$ is reported. The $k$-values distribution for the $Sr_3Ru_2O_7$ SPC [inset of Fig. 1(a)] is not a perfect Gaussian curve centered about $k=1.33$, as expected for a nominally pure $Sr_3Ru_2O_7$. The curve (guide to the eyes) indicates that the distribution is not symmetric with a tail toward higher $k$ values, indicating the presence of other homologs with $k>1.33$, i.e., $Sr_4Ru_3O_{10}$ ($k=1.5$) and $SrRuO_3$ ($k=2$). In contrast, the $k$ distribution corresponding to the $Sr_3Ru_2O_7$ EC [inset of Fig. 1(b)] is a quasisymmetric Gaussian, whose mean value and standard deviation are $\langle k \rangle = 1.33$ and $\sigma=0.01$, in reasonable agreement with the $k$ value of a $Sr_3Ru_2O_7$ SPC, indicating a minute contribution of dispersed $Sr_2RuO_4$ ($k=1$). In fact, a detailed EDS analysis of the clusters reveals a Sr:Ru:O=2:1:4 local chemical composition which justifies the shift of the mean $k$ value toward lower values. In addition, the precipitates embedded in the cluster matrix have a Ru-rich chemical composition but their contribution to the mean $k$ value is negligible due to their small volume fraction. This result is representative of all our $Sr_3Ru_2O_7$ SPC and $Sr_3Ru_2O_7$-$Sr_2RuO_4$ EC measured samples. The EDS data and the morphological analysis clearly show that the slight decrease in $k$ can be related to $Sr_2RuO_4$ clusters which are present in a very small amount and are randomly distributed over long distances. To rule out the presence of intergrowths of other R-P homologs not revealed by SEM/EDS, a detailed investigation at atomic scale is mandatory. For this purpose, the nanostructures of the two systems have been explored by TEM. Thin foils of approximately 100 nm thickness were extracted by focused ion beam "lift-out" procedure from the $Sr_3Ru_2O_7$ SPC and from the $Sr_3Ru_2O_7$ domain of the EC. Our analysis revealed profound differences between the two systems. The high-resolution TEM (HRTEM) investigation on the $Sr_3Ru_2O_7$ SPC showed that a fair proportion of the crystal has a disorder typical of intergrowths. As shown in the micrographs of Fig. 2 taken with the electron beam parallel to the [010] direction, such planar faults appear as embedded regions (enlightened by the dash-edged red boxes) with different atomic-layer stacking.

A diffuse dark contrast is associated with these areas, indicating the presence of strain. The inset of Fig. 2(a), in which a zoom-in of the defective region is displayed, shows that most of such phases are thin slabs of $SrRuO_3$ intercalating in the $Sr_3Ru_2O_7$ matrix, as enlightened by the dash-edged

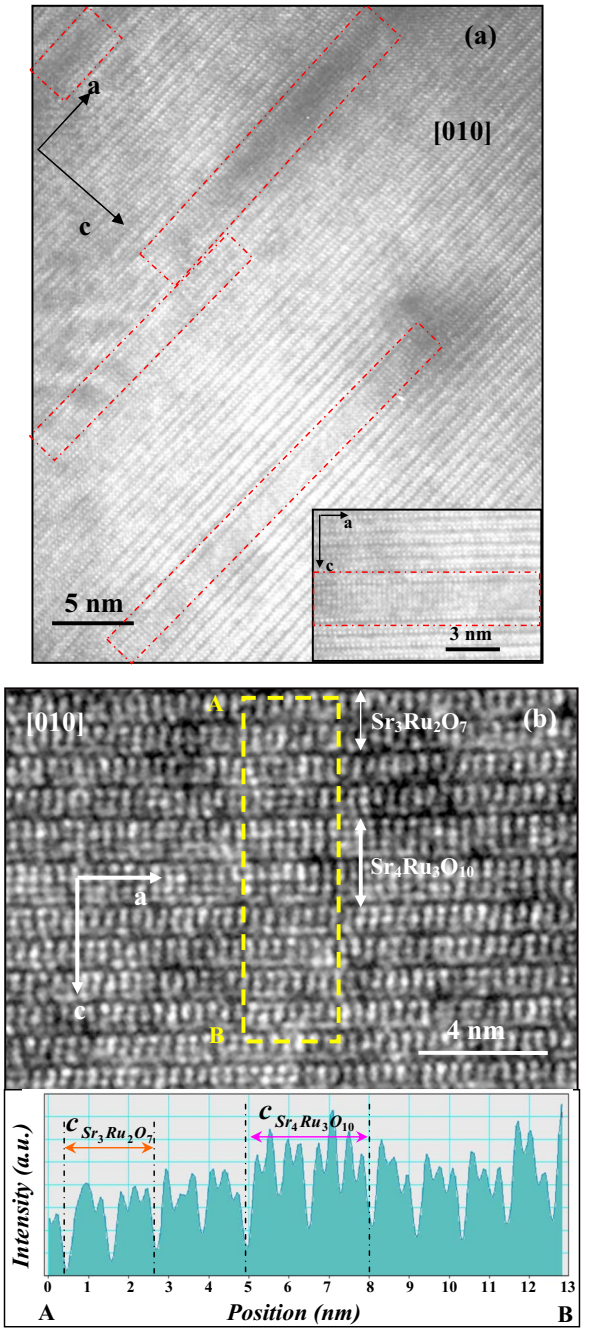


FIG. 2. (Color online) HRTEM micrographs of a $Sr_3Ru_2O_7$ SPC taken in the [010] zone axis: in (a) intergrowths of $SrRuO_3$ slabs intercalating within the $Sr_3Ru_2O_7$ matrix and associated with a diffuse dark contrast are shown (dash-edged red regions illustrated at higher resolution in the inset); in (b) isolated one unit-cell-thick layers of $Sr_4Ru_3O_{10}$ dispersed in the $Sr_3Ru_2O_7$ matrix and intensity profile taken integrating over the dash-edged box in which the $c$-axis parameters of $Sr_4Ru_3O_{10}$ and $Sr_3Ru_2O_7$ are quantified.

red box where the typical $SrRuO_3$ stacking can be discerned. Moreover, randomly distributed one unit-cell and half unit-cell-thick layers of $Sr_4Ru_3O_{10}$ are seen. In Fig. 2(b), the case of one unit cell of $Sr_4Ru_3O_{10}$ intercalating in the $Sr_3Ru_2O_7$ matrix is displayed. By the intensity profile, taken integrating over the dashed-edged area, the $c$-axis parameters corresponding to $Sr_3Ru_2O_7$ and $Sr_4Ru_3O_{10}$ are quantified in

$c_{Sr_3Ru_2O_7} \sim 2.1$ nm and $c_{Sr_4Ru_3O_{10}} \sim 2.9$ nm, respectively. These values are in good agreement with the *c*-axis values reported for $Sr_3Ru_2O_7$ (Refs. 24 and 25) and $Sr_4Ru_3O_{10}$.[26] On the contrary, the $Sr_3Ru_2O_7$ domain of the EC is perfectly ordered over large regions: neither intergrowths nor strain are observed in all the imaged areas over distances of more than 50 nm along the *c* direction [see Fig. 3(a)].

The HRTEM micrograph taken in the [010] zone axis of Fig. 3(b) shows no sizeable changes in the atom arrangement within the sample. In the intensity profile taken integrating over the dashed-edged region indicated in Fig. 3(b), the ~2-nm-long periodicity corresponds to the *c*-axis value of the $Sr_3Ru_2O_7$ phase. Only occasionally the investigation revealed the presence of layered defects interpreted as $Sr_2RuO_4$ layers in the $Sr_3Ru_2O_7$ matrix.[18] The volume fraction of these layers is extremely small in all the analyzed samples, as confirmed by selected-area electron diffraction (SAED). The typical electron-diffraction patterns of the $Sr_3Ru_2O_7$ SPC and of the $Sr_3Ru_2O_7$ domain of the EC are shown in Figs. 4(a) and 4(b), respectively. The analysis on the $Sr_3Ru_2O_7$ SPC [Fig. 4(a)] revealed the presence of both diffuse streaks along the *c* axis and extra spots in addition to the spots of the double-layered $Sr_3Ru_2O_7$ structure.

The stronger intensity of the $Sr_3Ru_2O_7$ spots indicates an overriding $Sr_3Ru_2O_7$ ordered volume in the sample. The additional spots are the characteristic reflections of the orthorhombic $Sr_4Ru_3O_{10}$ in the [010] zone axis. The presence of diffuse streaks running through the fundamental spots is characteristic of a two-dimensional lattice defect on the *a*-*b* plane due to the presence of the intergrowths. On the contrary, the SAED investigations performed on the $Sr_3Ru_2O_7$ domain of the EC [Fig. 4(b)] revealed only the characteristic spots of the $Sr_3Ru_2O_7$ phase. The above remarks underscore the higher purity of the $Sr_3Ru_2O_7$ domain of the EC in which no atomically layered spurious phases are seen except for intergrowths of $Sr_2RuO_4$ occurring in very localized regions with poorly ordered volume to yield detectable spots in either XRD or electron diffraction. The statistics carried out on several representative regions showed that the total volume fraction of the $Sr_2RuO_4$ intergrowths is less than 5% of the imaged volume. The higher purity of the $Sr_3Ru_2O_7$ domain of the EC compared to $Sr_3Ru_2O_7$ SPC, ascertained at atomic scale by TEM, is representative of the bulk samples, as confirmed by the magnetic measurements. Indeed, VSM measurements of tens of $Sr_3Ru_2O_7$ SPC and $Sr_3Ru_2O_7$-$Sr_2RuO_4$ EC revealed most of the eutectic samples have a significantly higher phase purity compared to $Sr_3Ru_2O_7$ SPC.

The susceptibility ($\chi = M/H_0$) (where *M* is the magnetization and $H_0$ the external magnetic field) versus temperature (*T*) measured on the $Sr_3Ru_2O_7$ SPC and the $Sr_3Ru_2O_7$-$Sr_2RuO_4$ EC are shown in Figs. 5(a) and 5(b), respectively. The curves were obtained in zero-field-cooling mode (ZFC, rightward orange arrow) and in field-cooling mode (FC, leftward orange arrow) applying magnetic fields at 50 Oe, and 3 and 10 kOe parallel to the *a*-*b* planes. At high field ($H_0 > 3$ kOe), in both crystals the susceptibilities are reversible and a maximum in the susceptibility is observed at about 16 K, typical of the $Sr_3Ru_2O_7$ phase.[13] As shown in the inset of Fig. 5(b), a large difference can be observed between the susceptibilities at 50 Oe measured on

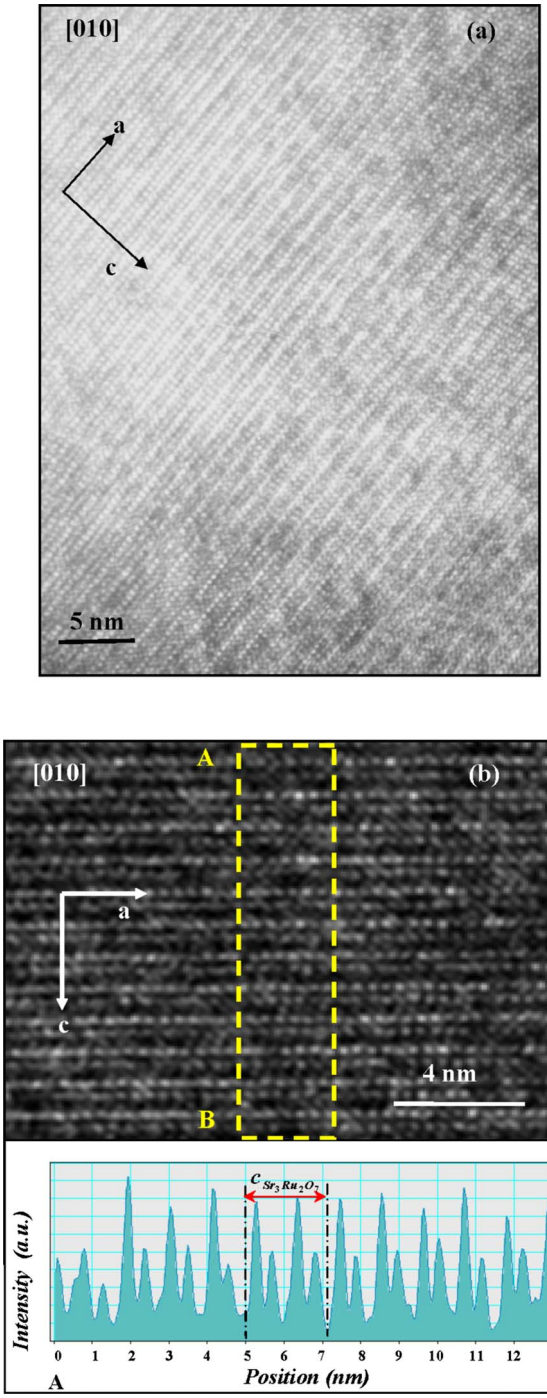


FIG. 3. (Color online) HRTEM micrographs in the [010] zone axis showing the well-ordered atom arrangement of the $Sr_3Ru_2O_7$ region of the eutectic. The *c*-axis parameter of $Sr_3Ru_2O_7$ [quantified by the intensity profile taken on the dash-edged box in (b)] is constant all over the sample.

the SPC and EC. In the SPC, the susceptibility displays two sharp enhancements at about 170 and 100 K, as emphasized by the blue and magenta arrows in the inset of Fig. 5(a), with a maximum around 16 K occurring in the ZFC branch. Moreover, below $T = 170$ K, the $\chi$ curve shows an irreversible behavior, questioning the occurrence of additional ferromagnetic phases within the crystal. Taking into account the

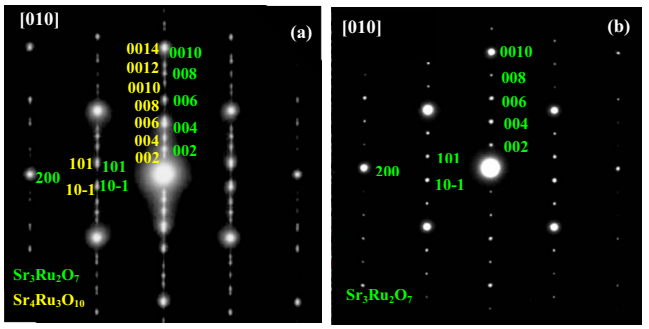


FIG. 4. (Color online) Selected-area electron-diffraction pattern in the [010] zone axis of (a) the $Sr_3Ru_2O_7$ single-phase crystals (b) the $Sr_3Ru_2O_7$ region of the eutectic. The pattern of figure (a) indicates the presence of $Sr_4Ru_3O_{10}$ intergrowths within the $Sr_3Ru_2O_7$ matrix. The reflections corresponding to $Sr_3Ru_2O_7$ (green) and $Sr_4Ru_3O_{10}$ (yellow) have been indexed assuming a tetragonal $I4/mmm$ (Refs. 24 and 25) and $Pbam$ (Ref. 26), respectively.

TEM and SEM data, these enhancements can be related to the $SrRuO_3$ and $Sr_4Ru_3O_{10}$ intergrowths. Moreover, the susceptibility curves measured below 170 K show a strong dependence on the applied magnetic field. In particular, $\chi$ measured below 35 K at 50 Oe is 50 times greater than its values at 10 kOe. The reversible behavior of the susceptibility, observed at higher field, is due to the paramagnetic fraction of the crystal, since the magnetization of the ferromagnetic phases is saturated. On the contrary, in the $Sr_3Ru_2O_7$-$Sr_2RuO_4$ EC, the susceptibility curves do not show any magnetic transition at about 170 K, ruling out the occurrence of $SrRuO_3$ within the eutectic. Moreover, the experimental values in the EC are nearly five times lower than the susceptibility measured at 10 kOe in the SPC and the susceptibility slightly depends on the applied magnetic field, as expected for a paramagnet with a small amount of ferromagnetic inclusions. Indeed, the $\chi$ measured at 50 Oe increases at 95 K with an irreversible behavior at $T<90$ K underlining the occurrence of a minute volume fraction of $Sr_4Ru_3O_{10}$ in the EC. Nevertheless, its effect on the susceptibility is very slight with respect to the analogs curves measured on SPC. From the above results, we conclude that the presence of ferromagnetic $Sr_4Ru_3O_{10}$ intergrowths in EC is very diluted, in a full agreement with all the structural layout. The higher purity of the $Sr_3Ru_2O_7$ domain of the EC, ascertained by TEM and by magnetic measurements, can be strictly related to the mechanism of the eutectic growth.[27] The lamellar eutectic structure is a consequence of the cooperative growth of two components accompanied by an atomic diffusion in front of the solid/liquid interface. In case of the $Sr_3Ru_2O_7$-$Sr_2RuO_4$ EC growth, at the steady state of the solidification, the mean $k$ value in the liquid nearby the solid/liquid interface is about 1.2. The solidification of the $Sr_2RuO_4$ phase ($k=1$) in front of the solid $Sr_2RuO_4$ seed leads to the increase in the local Ru concentration in the liquid. Analogously, the solidification of the $Sr_3Ru_2O_7$ phase occurs at the expenses of the mean $k$ value of the liquid which therefore tends to be lower than $k_f=1.2$ in front of the $Sr_3Ru_2O_7$ seed (leading, as a consequence, to an increase of the Sr concentration in the liquid). Therefore, the cooperative growth of the $Sr_3Ru_2O_7$ and $Sr_2RuO_4$ lamellae is accompanied by a Ru diffusion from the liquid in front of the $Sr_2RuO_4$ phase toward the region in front of the $Sr_3Ru_2O_7$, and by a Sr diffusion in the opposite direction. These driving forces tip the balance of the Sr and Ru concentration in front of the two solid phases, determining the lamellar thickness of the two phases. Furthermore, since in the eutectic solidification the $Sr_3Ru_2O_7$ crystal ($k=1.33$) is grown starting from a Ru-poor liquid ($k=1.2$), the formation of R-P phases with $k>1.33$, i.e., $Sr_4Ru_3O_{10}$ and $SrRuO_3$, is inhibited. On the contrary, during the single-phase crystal growth, the initial Ru excess ($k>1.33$), not evaporating during the growth, gives rise to spurious phases with $k>1.33$. Therefore, the occurrence of planar faults of $Sr_4Ru_3O_{10}$ and $SrRuO_3$ in $Sr_3Ru_2O_7$ SPC is due to the narrow region of the chemical phase diagram in which single-phase samples can be grown and of the unbalanced Ru off-stoichiometry during the growth. The presence of finite slabs of intergrowth having different atomic-layer stacking compared to the surrounding matrix, involves the occurrence of structural strain at the slab edges. This feature is shown in Fig. 2(a), where the difference between the $c$-axis parameters between the embedded $SrRuO_3$ slabs and the $Sr_3Ru_2O_7$ SPC

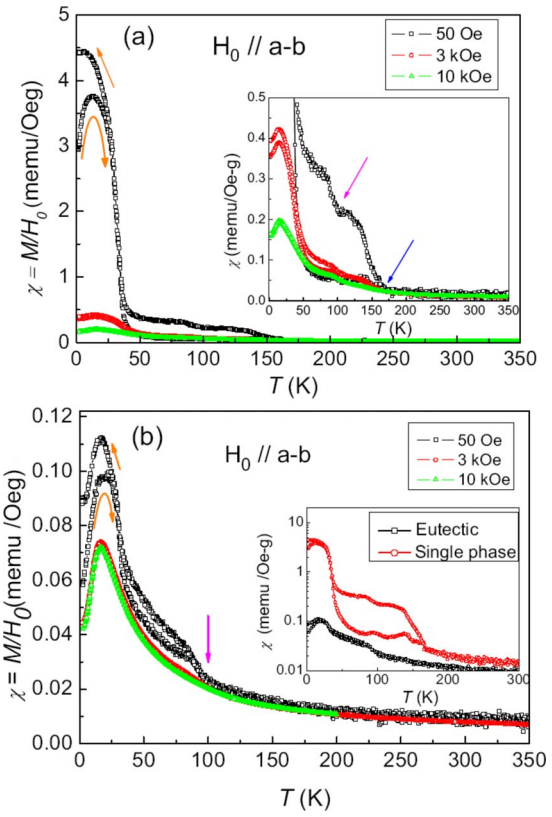


FIG. 5. (Color online) Susceptibilities $\chi=(M/H_0)$ versus temperature measured on (a) a $Sr_3Ru_2O_7$ SPC and on (b) a $Sr_3Ru_2O_7$-$Sr_2RuO_4$ eutectic crystal at 50 Oe, and 3 and 10 kOe magnetic field parallel to the $a$-$b$ planes. In the inset of (a), a zoom of the susceptibility curves measured on the single-phase sample. In the inset of (b) the susceptibility curves at 50 Oe of both crystals are displayed in semilog scale. The rightward and leftward orange arrows indicate the ZFC and FC curves, respectively. The blue and magenta arrows indicate the magnetic transition of the $SrRuO_3$ and the $Sr_4Ru_3O_{10}$ phases, respectively.

matrix leads to the occurrence of strain which appears as a diffuse dark contrast.

## IV. CONCLUSION

We have shown that $Sr_3Ru_2O_7$ in $Sr_3Ru_2O_7$-$Sr_2RuO_4$ eutectic crystals can be grown with higher quality than $Sr_3Ru_2O_7$ single-phase crystals. Indeed the HRTEM on $Sr_3Ru_2O_7$ SPC revealed the presence of atomically layered $Sr_4Ru_3O_{10}$ and $SrRuO_3$ within the $Sr_3Ru_2O_7$ matrix associated with strain and randomly dispersed $Sr_2RuO_4$ clusters. On the contrary, $Sr_3Ru_2O_7$ grown via eutectic solidification showed a much more ordered microstructure with a small amount of randomly dispersed $Sr_2RuO_4$ clusters and only a very diluted presence of layered $Sr_2RuO_4$. The profound difference in the nanostructures of the two systems is reflected in their magnetic behavior: susceptibility versus temperature curves measured on $Sr_3Ru_2O_7$ SPC in low magnetic fields revealed two additional magnetic transitions at 170 and 100 K, compatible with the presence of $SrRuO_3$ and $Sr_4Ru_3O_{10}$, respectively. The same measurement performed on the eutectic material confirmed that the $Sr_3Ru_2O_7$ domain of the EC have less impurities than the $Sr_3Ru_2O_7$ SPC. This result is particularly relevant if we consider that resistivity versus temperature measurements performed on these crystals show that the two systems have comparable residual resistivity values.[28] Due to the higher purity, the $Sr_3Ru_2O_7$ grown via eutectic solidification is the best candidate to study the intrinsic transport/magnetic properties of the $Sr_3Ru_2O_7$ phase. Our results show that the eutectic solidification can be a fruitful way to grow high-quality samples of strontium ruthenates. Because of the high similarities between these materials and other polymorphic oxides, these findings can be considered as representative of a wide class of materials and therefore applicable to the eutectic growth of other anisotropic oxides systems. Indeed in eutectic crystals, where two phases form alternating domains, the solidification process tends to preserve the coherence of each domain which can grow with a considerably lower amount of impurities. The eutectic solidification therefore promotes a morphology of the phases which allows the extraction of embedded crystals using recently developed techniques for measurements on local scale. This enables the investigation of fundamental properties of each crystal structure and also future applications spurred by the particular properties of the crystals.

## ACKNOWLEDGMENTS

The work presented here was partly supported through SSF program OXIDE, a VR grant, and the Swedish National Graduate School of Material Science. Funding for the SEM laboratory at Chalmers from the Knut and Alice Wallenberg Foundation and for the combined FIB SEM from VR is gratefully acknowledged. Moreover, R.C. acknowledges the Swedish Institute, the Blanceflor Boncompagni-Lodovisi Foundation, and the "Angelo della Riccia" Foundation, for financing her research period at the Chalmers University of Technology. R.C. also acknowledges the ESF activity Thin Films for Novel Oxide Devices (THIOX), within the Exchange Grants program.

*Present address: CNR-INFM TASC National Laboratory, Area Science Park, Basovizza S.S. 14 Km 163.5, 34012 Trieste, Italy; ciancio@tasc.infm.it

[1] G. Cao, C. S. Alexander, S. McCall, J. E. Crow, and R. P. Guertin, Mater. Sci. Eng., B **63**, 76 (1999).
[2] A. P. Mackenzie and Y. Maeno, Rev. Mod. Phys. **75**, 657 (2003).
[3] S. Nakatsuji and Y. Maeno, Phys. Rev. Lett. **84**, 2666 (2000).
[4] S. A. Grigera, P. Gegenwart, R. A. Borzi, F. Weickert, A. J. Schofield, R. S. Perry, T. Tayama, T. Sakakibara, Y. Maeno, A. G. Green, and A. P. Mackenzie, Science **306**, 1154 (2004).
[5] A. P. Mackenzie, R. K. W. Haselwimmer, A. W. Tyler, G. G. Lonzarich, Y. Mori, S. Nishizaki, and Y. Maeno, Phys. Rev. Lett. **80**, 161 (1998).
[6] Z. Q. Mao, Y. Maeno, and H. Fukazawa, Mater. Res. Bull. **35**, 1813 (2000).
[7] K. T. Jacob, K. T. Lwin, and Y. Waseda, Mater. Sci. Eng., B **103**, 152 (2003).
[8] S. A. Grigera, R. S. Perry, A. J. Schofield, M. Chiao, S. R. Julian, G. G. Lonzarich, S. I. Ikeda, Y. Maeno, A. J. Millis, and A. P. Mackenzie, Science **294**, 329 (2001).
[9] R. S. Perry, L. M. Galvin, S. A. Grigera, L. Capogna, A. J. Schofield, A. P. Mackenzie, M. Chiao, S. R. Julian, S. I. Ikeda, S. Nakatsuji, Y. Maeno, and C. Pfleiderer, Phys. Rev. Lett. **86**, 2661 (2001).
[10] R. S. Perry, K. Kitagawa, S. A. Grigera, R. A. Borzi, A. P. Mackenzie, K. Ishida, and Y. Maeno, Phys. Rev. Lett. **92**, 166602 (2004).
[11] R. J. Cava, H. W. Zandbergen, J. J. Krajewski, W. F. Peck, Jr., B. Batlogg, S. Carter, R. M. Fleming, O. Zhou, and L. W. Rupp, Jr., J. Solid State Chem. **116**, 141 (1995).
[12] G. Cao, S. McCall, and J. E. Crow, Phys. Rev. B **55**, R672 (1997).
[13] S. I. Ikeda, Y. Maeno, S. Nakatsuji, M. Kosaka, and Y. Uwatoko, Phys. Rev. B **62**, R6089 (2000).
[14] R. Mathieu, A. Asamitsu, Y. Kaneko, J. P. He, X. Z. Yu, R. Kumai, Y. Onose, N. Takeshita, T. Arima, H. Takagi, and Y. Tokura, Phys. Rev. B **72**, 092404 (2005).
[15] R. Fittipaldi, A. Vecchione, S. Fusanobori, K. Takizawa, H. Yaguchi, J. Hooper, R. S. Perry, and Y. Maeno, J. Cryst. Growth **271**, 152 (2004).
[16] J. Hooper, M. Zhou, Z. Q. Mao, Y. Liu, R. Perry, and Y. Maeno, Phys. Rev. B **73**, 132510 (2006).
[17] S. Kittaka, S. Fusanobori, S. Yonezawa, H. Yaguchi, Y. Maeno, R. Fittipaldi, and A. Vecchione, Phys. Rev. B **77**, 214511 (2008).
[18] R. Fittipaldi, A. Vecchione, R. Ciancio, S. Pace, M. Cuoco, D. Stornaiuolo, D. Born, F. Tafuri, E. Olsson, S. Kittaka, H. Yaguchi, and Y. Maeno, Europhys. Lett. **83**, 27007 (2008).
[19] T. Williams, F. Lichtenberg, A. Relier, and G. Bednorz, Mater. Res. Bull. **26**, 763 (1991).

[20] W. Tian, J. H. Haeni, D. G. Schlom, E. Hutchinson, B. L. Sheu, M. M. Rosario, P. Schiffer, Y. Liu, M. A. Zurbuchen, and X. Q. Pan, Appl. Phys. Lett. **90**, 022507 (2007).
[21] C. N. R. Rao, Bull. Mater. Sci. **7**, 155 (1985).
[22] M. Yu. Kameneva, L. P. Kozeeva, N. V. Podberezskaya, D. Yu. Naumov, N. V. Kurat'eva, and V. E. Fedorov, Inorg. Mater. **43**, 845 (2007).
[23] A. Berger, R. M. Osgood III, J. S. Jiang, D. J. Miller, J. F. Mitchell, and S. D. Bader, Mater. Sci. Eng., B **63**, 133 (1999).
[24] Q. Huang, J. W. Lynn, R. W. Erwin, J. Jarupatrakorn, and R. J. Cava, Phys. Rev. B **58**, 8515 (1998).
[25] H. Shaked, J. D. Jorgensen, O. Chmaissem, S. Ikeda, and Y. Maeno, J. Solid State Chem. **154**, 361 (2000).
[26] M. K. Crawford, R. L. Harlow, W. Marshall, Z. Li, G. Cao, R. L. Lindstrom, Q. Huang, and J. W. Lynn, Phys. Rev. B **65**, 214412 (2002).
[27] K. A. Jackson and J. D. Hunt, Trans. Metall. Soc. AIME **236**, 1129 (1966).
[28] S. Kittaka, S. Yonezawa, H. Yaguchi, Y. Maeno, R. Fittipaldi, A. Vecchione, J. F. Mercure, A. Gibbs, R. S. Perry, and A. P. Mackenzie, J. Phys.: Conf. Ser. **150**, 052113 (2009).